COMPARISON OF THE OXYGEN CONCENTRATION IN CZOCHRALSKI SILICON CRYSTAL OBTAINED BY A SIMPLE LUMPED-PARAMETER MODEL AND SOPHISTICATED 2D-3D SIMULATIONS

J. Friedrich[1], M. Trempa[1], H. Koch[1], F. Mosel[2], A. Mühe[2]
[1]Fraunhofer IISB, Schottkystr. 10, 91058 Erlangen, Germany
[2]PVA Crystal Growing Sytems GmbH, Im Westpark 10-12, 35435 Wettenberg, Germany
Email: jochen.friedrich@iisb.fraunhofer.de

ABSTRACT: In the present work a simple boundary layer model for the oxygen transport during Cz silicon crystal growth is revisited and extended by introducing classical scaling laws for the thicknesses of the different boundary layers at the crucible wall, at the free melt surface and at the solid-liquid interface. This lumped model is used to calculate the influence of crystal and crucible rotation on the oxygen transport during Cz growth of 100kg heavy silicon crystals with 210mm diameter in a 24" hot zone geometry. The results of this reduced order model are compared to results from sophisticated, coupled 2D-3D, global numerical simulations of the whole Cz puller. It is found that at a first glance the accuracy of the boundary layer model can be sufficient for certain coarse case studies. However, the boundary layer model hits quickly the wall, when a precise analysis of the oxygen transport is required. The root cause is believed to be the complex flow structure, which results from the combination of crystal and crucible rotation in the vicinity of the solid-liquid interface. For an accurate analysis of oxygen transport sophisticated simulations are indispensable.
Keywords: Convection; Computer simulation; Czochralski; Single Crystal Growth; Silicon

1 INTRODUCTION

Numerical modeling has become an essential tool for optimization and further development of the Cz process of Si mono-crystals for photovoltaic applications with respect to low oxygen concentrations. This is particularly true for large diameter growth processes as respective growth experiments are very expensive. This precise modeling approach is typically achieved by a combination of a global, quasi-stationary, axisymmetric model of the whole Cz puller with a local three-dimensional, time-dependent model of the melt-crystal-crucible region. Thereby, the usage of Large Eddy Simulation (LES) turbulence model is well established [1-9].

However, such numerical calculations, giving precisely high-fidelity spatiotemporal profiles of important process parameters such as oxygen distribution, temperature distribution, and flow profiles, take typically several weeks on a high performance cluster to complete. To get a quick estimation on the influence of process parameters on the crystal properties with reasonable accuracy, a reduced-order model would be desired where results can be obtained more or less within real time. Such lumped parameter model would also allow understanding easier the phenomena e.g. occurring in the melt, if the main physical mechanisms are considered.

Such reduced order models were typically developed in the 1970ies and 1980ies when numerical simulation of the Cz process was in an infancy stage. One example is the boundary layer model for the oxygen transport published by Carlberg et al. [10] and Hoshikawa et al. [11]. With increasing accuracy of numerical simulations these reduced-order models have slided into obscurity. Therefore, it is unclear whether lumped-parameter models are able to predict the influence of different process parameter on the oxygen transport for large diameter Cz silicon crystal growth with almost the same accuracy than highly sophisticated, time consuming 2D-3D simulations.

Therefore, in this work we used a further developed version of the boundary layer model of [10, 11] to calculate the influence of crystal and crucible rotation on the oxygen transport. The results of this reduced-order model will be compared to results obtained by coupled 2D-3D simulations.

2 COUPLED 2D-3D NUMERICAL SIMULATIONS

We performed coupled 2D-3D simulations of the heat and oxygen transport during growth of Si crystals with 210mm diameter and a weight of 190kg in a 24" (diameter of the silica crucible) hot zone. In the 2D-3D model the convective heat and oxygen transfer are computed by a time-dependent 3D-LES model [5, 6]. Temperature, melt velocities and oxygen concentration are averaged azimuthally and in time, and a turbulent heat flux is calculated form the observed fluctuations of temperature and velocity. These average values plus the turbulent heat fluxes are then imported into a Reynolds averaged form of the temperature equation inside the 2D-model, in which the temperature field as well as the SiO evaporated from the melt surface in the whole Cz puller geometry is calculated. The details of the 2D-3D model can be found in [5, 6, 12]. The 2D-3D model was already validated by comparison to data from Direct Numerical Simulation as well as by comparison to experimental data with respect to the shape of the solid-liquid interface and oxygen distribution in large diameter Si Cz crystals [5, 6].

3 THE REDUCED-ORDER MODEL

Our approach in developing a reduced-order model begins with the assumption of a well-mixed melt region, thus eliminating spatial variation of dissolved oxygen from the crucible. Due to strong flows from the combination of Rayleigh-Bernard convection with azimuthal crystal and/or crucible rotation, adequate mixing from turbulence is assumed. Fluxes of oxygen in and out are estimated as simple linear Fickian diffusion across boundary layers of defined width as originally proposed by [10, 11] (see Figure 1).

The basic variables of interest are defined in Table 1. In general, subscripts of c, s, m, and x will refer to crucible, free melt surface, melt volume, and crystal, respectively. The material properties of silicon used in the present work can be found in [5].

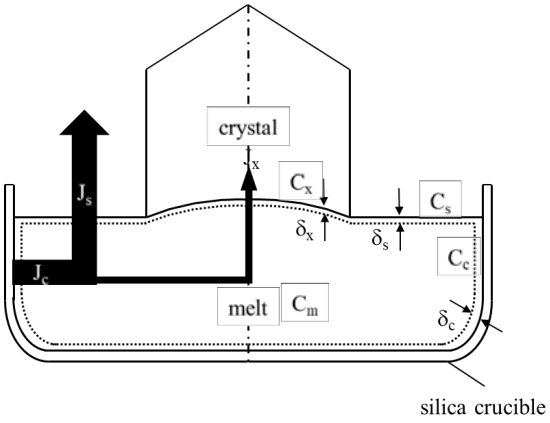

Figure 1: Cartoon of basic mass flows.

Vari-able	Description
C_c	Equilibrium concentration at crucible wall
C_m	Solute concentration in the melt volume
C_s	Solute concentration at the free melt surface
C_x	Solute concentration at the s/l interface
A_c	Contact area between melt and crucible wall
A_s	Area of free melt surface
A_x	Area of s/l interface
D	Diffusion coefficient
r_c	Crucible radius
r_x	Crystal radius
δ_i	Solute boundary layer thickness
$\dot{n}_i$	Molar flow rate
J_i	Molar flux
ω_i	Angular velocity

Table 1: Basic variables of the boundary layer model. In general, subscripts of c, s, m, and x will refer to crucible, free melt surface, melt volume, and crystal, respectively.

3.1 Mass fluxes J_i at crucible wall, free surface and solid/liquid interface

We define the molar oxygen fluxes from the crucible into the melt, out of the free melt surface, and into the crystal as $\dot{n}_c$, $\dot{n}_s$, and $\dot{n}_x$, respectively. Thus, the flux of oxygen into the melt from the crucible wall is given by

$$\dot{n}_c = J_c A_c \qquad \text{eq. 1}$$
$$J_c = \frac{D}{\delta_c}(C_c - C_m) \qquad \text{eq. 2}$$

At the melt surface the flux of oxygen from the melt into the gas ambient is defined as

$$\dot{n}_s = J_s A_s \qquad \text{eq. 3}$$
$$J_s = \frac{D}{\delta_s}(C_m - C_s) \qquad \text{eq. 4}$$

We assume that we have an ideal transport of SiO from the melt surface into the ambient gas. Therefore, all SiO formed at the surface is immediately removed and the oxygen concentration at the melt surface C_s approaches zero. This assumption is also used in our 2D-3D model, because it has been proven that the interaction of the gas flow with the melt flow can be neglected for the given puller geometry and process parameters.

At the solid-liquid interface the flux of oxygen out of the melt is given by

$$\dot{n}_x = J_x A_x \qquad \text{eq. 5}$$
$$J_x = k_{eff} V C_m \qquad \text{eq. 6}$$

Here we use the Burton-Prim-Schlichter (BPS) model to derive the effective segregation coefficient k_{eff}.

$$k_{eff} = \frac{k}{k+(1-k)\exp(-\frac{V\delta_x}{D})} \qquad \text{eq. 7}$$

δ_x is the solute boundary layer at the solid-liquid interface, V the pull rate. δ_x can be approximated by the model for a rotating disk, which gives [13]:

$$\delta_x = 1.6 D^{1/3} \upsilon^{1/6} {\omega_x}^{-1/2} \qquad \text{eq. 8}$$

3.2 Mass balance

Because of slow growth rates, we assume a pseudo-steady concentration inside the melt volume. The mass balance then becomes:

$$\frac{\mathrm{dn_m}}{\mathrm{dt}} = 0 = \mathrm{J_c A_c} - \mathrm{J_s A_s} - \mathrm{J_x A_x} \qquad \text{eq. 9}$$

And solving for C_m gives

$$C_m = \frac{1}{1+\frac{A_s\delta_c}{A_c\delta_s}+\frac{A_x\delta_c}{A_c D}V\,k_{eff}} C_c \qquad \text{eq. 10}$$

If we neglect the bending of the solid-liquid interface, then the areas A_i are all known from the crystal and crucible geometry and the initial melt mass. Also the equilibrium oxygen concentration at the crucible wall C_c is known. Figure 2 shows the temperature dependence of the oxygen equilibrium concentration published from several authors [14-17]. Most papers within the last ten years are using the curve from Togawa et al. [14] as boundary condition in their numerical simulations. We apply also this curve in our coupled 2D-3D approach as well as in our lumped model. However, in the lumped model we neglect completely the temperature dependence and assume a constant value of C_c=2x10^{18}cm^{-3}.

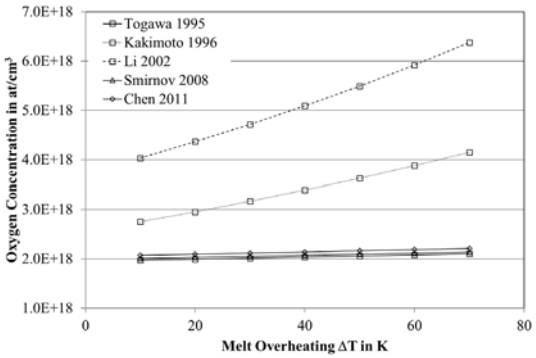

Figure 2: Equilibrium oxygen concentration at the crucible wall C_c versus melt overheating ΔT published by several authors [14-17].

A priori, the solute boundary layer thickness at the crucible, at the melt surface and at the solid-liquid interface are unknown, but can be estimated from transport scaling relationships and process parameters for the momentum boundary layers. Thereby, the Schmid number Sc = (ν/D) is used to approximate the thickness of the solutal boundary layer δ_i from the momentum boundary layer δ_i' [18] which is marked by a prime further on.

$$\delta_i = 2.4 * Sc^{-1/3}\delta_i' \qquad \text{eq. 11}$$

To estimate $\delta c'$, we turn to an analysis of King et al. [19]. They investigated the different flow regimes in rotating Ralyeigh-Benard configurations in dependence on the Ekman number Ek and Rayleigh number Ra which are defined for the present work as follows:

$$Ek = \frac{\nu}{2\omega_c {r_c}^2} \qquad \text{eq. 12}$$

$$Ra = \frac{\beta g \Delta T {r_c}^3 (\frac{h}{r_c})}{\kappa \nu} = Gr * Pr \qquad \text{eq. 13}$$

with volumetric expansion coefficient β, melt height h, crucible radius r_c, crucible rotation ω_c, melt overheating ΔT, kinematic viscosity ν, thermal diffusivity κ, Grashof number Gr, and Prandtl number Pr= κ/ ν.

King et al. [19] found that for geostrophic conditions ($Ra \cdot Ek^{3/2} < 10$) the momentum boundary layer thickness follows a scaling relationship with the Ekman number Ek:

$$\delta_c' = 3Ek^{1/2} r_c \qquad \text{eq. 14}$$

This criterion for geostrophic flow is fulfilled for the present Cz set-up ($0.01 < Ra \cdot Ek^{3/2} < 0.1$), therefore eq. 14 should be valid. However, to check this assumption we used also the alternate estimation for non-rotating Rayleigh-Bernard convection [19], which is possible by the Grashof number, Gr.

$$\delta_c' = Gr^{-1/4} r_c \qquad \text{eq. 15}$$

For the free surface, we utilize the analysis of [20]. The thickness of momentum boundary layer associated with Marangoni flow over the free surface is found to follow the following relationship with the Marangoni number Ma. The relevant length scale here is the distance between the crucible wall and the crystal, or $r_c - r_x$. The Marangoni number is defined as

$$Ma = \frac{-\left(\frac{\partial \sigma}{\delta T}\right)\Delta T (r_c - r_x)}{\rho \nu^2} \qquad \text{eq. 16}$$

with density ρ, and temperature dependence of surface tension $\frac{\partial \sigma}{\delta T}$. Accordingly, the momentum boundary layer thickness at the free melt surface becomes:

$$\delta_s' = Ma^{-1/3}(r_c - r_x) \qquad \text{eq. 17}$$

Finally, we get the following expression for the oxygen concentration by using the momentum instead of the solute boundary layer thicknesses.

$$C_m = \frac{1}{1 + \frac{A_s \delta_c'}{A_c \delta_s'} + \frac{A_x}{A_c (D/V)} \frac{\delta_c'}{Sc^{1/3}} 2.4\, k_{eff}} C_c \qquad \text{eq. 18}$$

4 RESULTS AND DISCUSSION

4.1 Influence of melt overheating

In eq. 18 all parameters are known except the melt overheating ΔT, which is needed to calculate the Grashof- and Marangoni-number. Figure 3 and Figure 4 show the dependence of the overheating ΔT on the crucible rotation ω_c and crystal rotation ω_x for different body lengths (resp. solidified fractions g), obtained from our 2D-3D simulations. As already known from literature [21] the overheating increases with increasing crucible rotation, because the convective heat transport in the lateral direction is suppressed due to the higher Coriolis force for higher crucible rotation. The influence of crystal rotation is minor.

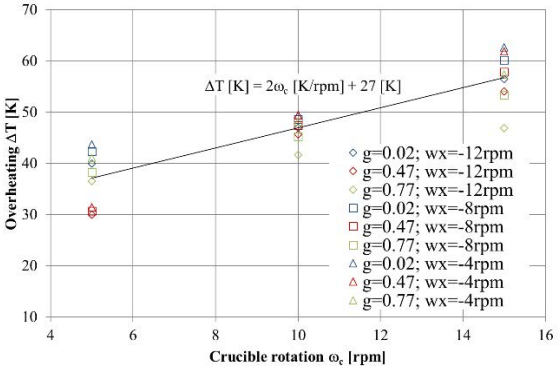

Figure 1: Melt overheating ΔT versus crucible rotation ω_c for different solidified fractions g and crystal rotations ω_x obtained from 2D-3D simulations.

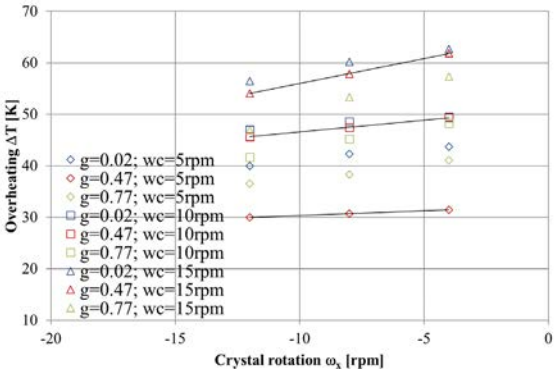

Figure 4: Melt overheating ΔT versus crystal rotation ω_x for different solidified fractions g and crucible rotations ω_c obtained from 2D-3D simulations.

In a first step, let us neglect J_x and consider J_c and J_s only. For a given crucible rotation the overheating decreases by less than 10K with increasing the crystal rotation, which means that the momentum boundary layer $\delta s'$ increases, the term $A_s \delta c'/ A_c \delta s'$ decreases and therefore, the oxygen concentration increases by less than 3% according to the lumped model. Therefore, we consider only the dependence of the overheating ΔT on the crucible rotation, which can be expressed as follows when we apply a linear trend line to the data in Figure 3:

$$\Delta T \approx 27K + 2\omega_c [\frac{K}{rpm}] \qquad \text{eq. 19}$$

4.2 Importance of mass flux J_x

In a second step, we analyze the importance of the mass flux J_x. A priori, it is expected that most of the oxygen entering the melt over the crucible wall will evaporate as SiO from the melt surface [22], that means that the oxygen concentration depends strongly on the contact area A_c between melt and crucible and that J_x is small compared to J_s. The latter is equivalent that the third term in the denominator of eq. 18 is negligible. Figure 5 shows indeed that the oxygen concentration decreases with increasing

body length, because the contact area A_c decreases and thus, the denominator of eq. 18 increases. It is also obvious that the oxygen concentration will increase by less than 5% only when the mass flux J_x is not considered.

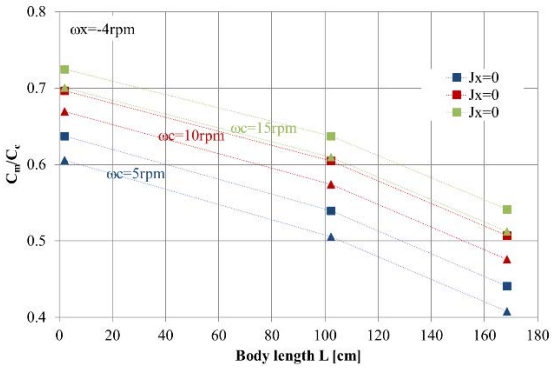

Figure 5: Normalized oxygen concentration C_m/C_c versus body length of the crystal for different crucible rotations ω_c at crystal rotation ω_x=-4rpm calculated by eq. 18 with eqs. 14, 17 and 19 w/o consideration of the mass flux J_x.

4.3 Influence of crucible rotation

In a further step, we compare the results of the boundary layer model with coupled 2D-3D simulations for varying crucible rotation and constant crystal rotation. In the boundary layer model, eq. 19 was used to calculate the melt overheating ΔT. Figure 6 shows the oxygen concentration in the crystal calculated by the boundary layer model and obtained from the 2D-3D simulations. The results of the boundary layer model are in qualitative agreement to the 2D-3D simulations when the Ekman number is used to determine the boundary layer thickness at the crucible wall (eq. 14). In this case, the well-known increase of oxygen concentration with increasing crucible rotation [22] is well represented. The root cause is the decreasing boundary layer thickness δ_c at the crucible wall with increasing crucible rotation, which results in an increase of the oxygen flux into the melt.

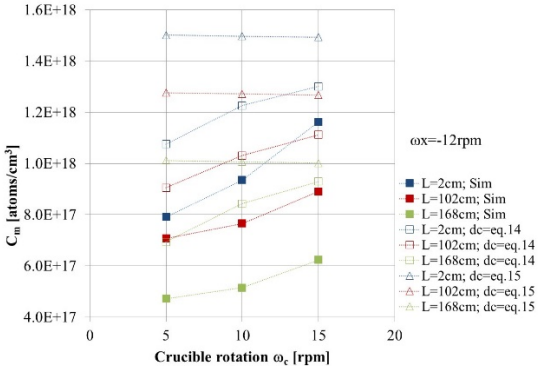

Figure 6: Oxygen concentration versus crucible rotation at constant crystal rotation (-12rpm) for different body lengths. Full squares represent the results of the simulations, open squares the results of the boundary layer model using eq. 14, open triangles the results of the boundary layer model using eq. 15.

On the other hand, when the boundary layer at the crucible wall is calculated by using the Grashof number (eq.15), no dependence of the oxygen concentration on the crucible rotation is found. This proofs that convection in the silicon melt represents a geostrophic flow under these conditions.

4.4 Influence of crystal rotation

In a last step, we compare the results of the boundary layer model with coupled 2D-3D simulations for constant crucible rotation and varying crystal rotation.

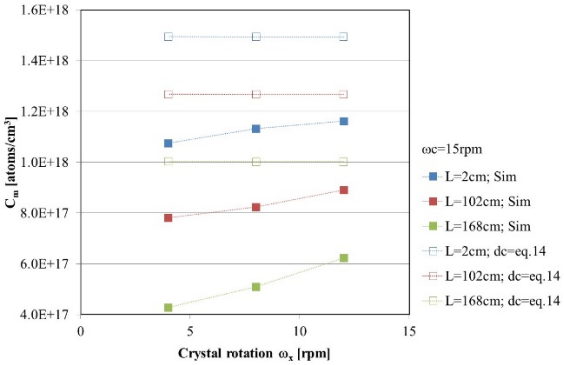

Figure 7: Oxygen concentration versus crystal rotation at constant crucible rotation (15rpm) for different body lengths. Full squares represent the results of the simulations, open squares the results of the boundary layer model using eq. 14.

From Figure 7 is obvious that the slight increase of the oxygen concentration with increasing crystal rotation in the 2D-3D simulation is not reproduced by the boundary layer model. Obviously, the influence of the crystal rotation is underestimated in the boundary layer model. In order to check whether this could be caused by the assumption of a flat interface in the boundary layer model we replaced the ideal area of the flat interface by the real area of the curved interface A_x, which we extracted from the 2D-3D simulations. In addition, we replaced the approximated melt overheating (eq. 19) by the values obtained from the simulation. However, there is almost no difference between these three cases. Thus, the complex flow structure itself is contributing much to the real oxygen transport, which is not represented in this very simple lumped parameter model.

5 CONCLUSIONS

The boundary layer model allows the calculation of the oxygen concentration at the touch of a button on a simple PC, whereas the coupled 2D-3D simulations take several weeks on a PC cluster. The comparison to the 2D-3D simulations shows that at a first glance the accuracy of the boundary layer model is sufficient for certain coarse case studies. Therefore, it can contribute to a quick and improved understanding about the oxygen transport during silicon Czochralski crystal growth, especially for beginners in crystal growth. Extensions of the model to take into account magnetic field effects or the influence of the interaction of melt and gas flow can be carried out easily as already shown in literature.

However, the boundary layer model hits quickly the wall, when a precise analysis of the oxygen transport is required. The root cause is believed the complex flow structure, which results from the combination of crystal and crucible rotation in the vicinity of the solid-liquid interface. For a better accuracy, it might be useful to consider several melt regions beneath the crystal in the model. However, it is assumed that too much data have to be extracted from the 2D-3D simulations which serve as input parameter for such improved boundary layer model.

This contradicts the charm of a lumped model.

Therefore, only first rough estimations can be made by using the boundary model. For more accurate treatments coupled 2D-3D simulations of the oxygen transport are indispensable.

6 ACKNOWLEDGEMENT

Our former colleague Dr. Thomas Jung is highly acknowledged for carrying out the 2D-3D simulations. We thank also Prof. Jeff J. Derby and Kerry Wang from the University of Minnesota for the fruitful discussion about the applicability of the lumped model. Research and development published in this work were part of the *CZ3003* project, which is funded partly by the German Federal Ministry for Economic Affairs and Energy (BMWI) under contract number 0324357A.

7 REFERENCES

[1] I. Yu. Evstratov, V. V. Kalaev, A. I. Zhmakin, Yu. N. Makarov, A. G. Abramov, N. G. Ivanov, E. M. Smirnov, E. Dornberger, J. Virbulis, E. Tomzig, W. von Ammon, Journal of Crystal Growth 230 (2001) 22-29

[2] D. P. Lukanin, V. V. Kalaev, Yu. N. Makarov, T. Wetzel, J. Virbulis, W. von Ammon, Journal of Crystal Growth 266 (2004) 20-27

[3] D. Smirnov, V.V. Kalaev, Journal of Crystal Growth 310(12) (2008) 2970-2976

[4] A. Krauze, N. Jekabsons, A. Muiznieks, A. Sabanskis, U. Lacis, Journal of Crystal Growth 312 (2010) 3225-3234

[5] T. Jung, J. Seebeck, J. Friedrich, Journal of Crystal Growth 368 (2013) 72–80

[6] J. Friedrich, T. Jung, M. Trempa, C. Reimann, A. Denisov, A. Muehe, Journal of Crystal Growth 524 (2019) 125-168

[7] J. Zhang, J.-C. Ren, D. Liu, Results in Physics 13 (2019) 102127

[8] R. Yokoyama, T. Nakamura, W. Sugimura, T. Ono, T. Fujiwara, K. Kakimoto, Journal of Crystal Growth 519 (2019) 77–83

[9] V. Kalaev, Journal of Crystal Growth 532 (2020) 125413

[10] T. Carlberg, T. B. King, A. F. Witt, J. Electrochem. Soc. 129/1 (1982) 189–193

[11] K. Hoshikawa, X. Huang, Materials Science and Engineering B 72(2–3) (2000) 73-79

[12] J. Fainberg, D. Vizman, J. Friedrich, G. Mueller, Journal of Crystal Growth 303(1) (2007) 124-134

[13] A. G. Ostrogorsky, G. Müller, Journal of Crystal Growth 121(4) (1992) 587-598

[14] S. Togawa, X. Huang, K. Izunome, K. Terashima, S. Kimura, Journal of Crystal Growth 148 (1–2) (1995) 70-78

[15] K. Kakimoto, K. Yi, M. Eguchi, Journal of Crystal Growth 163 (3) (1996) 238-242

[16] M. Li, Y. Li, N. Imaishi, T. Tsukada, Journal of Crystal Growth 234 (1) (2002) 32-46

[17] J. C. Chen, Y. Y. Teng, W. T. Wun, C. W. Lu, H. I. Chen, C. Y. Chen, C. Y., W. C. Lan, Journal of Crystal Growth 318(1) (2011) 318-323

[18] B. Vartak, A. Yeckel, J. J. Derby, Journal of Crystal Growth 283 (2005) 479–489

[19] E. M. King, S. Stellmach, and B. Buffett, Journal of Fluid Mechanics 717 (2013) 449-471

[20] Y. Okano, A. Hatano, A. Hirata, J. Electrochem. Eng. Jpn.22(4) (1989) 385-388

[21] D. Vizman, O. Gräbner, G. Müller, Journal of Crystal Growth 233 (2001) 687–698

[22] J. Friedrich, W. von Ammon, G. Müller, Czochralski Growth of Silicon Crystals, in: Handbook of Crystal Growth Vol. II. (Eds. T. Nishinaga, P. Rudolph) Elsevier (2015) 45–104